Seasonal forecast of South China Sea summer monsoon onset disturbed by the cold tongue La Niña in recent decade

Ning JIANG[1] and Congwen ZHU[*1]

[1] *State Key Laboratory of Severe Weather (LASW) and Institute of Climate System, Chinese Academy of Meteorological Sciences, Beijing 100081, China*

ABSTRACT

It has been suggested that a warm (cold) ENSO event in winter is mostly followed by the late (early) onset of the South China Sea (SCS) summer monsoon (SCSSM) in spring. Our results show this positive relationship, which is mainly determined by their phase correlation, has been broken under recent rapid global warming since 2011, due to the disturbance of cold tongue (CT) La Niña events. Different from canonical counterpart, the CT La Niña event is characterized by surface meridional wind divergences in the central-eastern equatorial Pacific, which can delay the SCSSM onset by the enhanced convections in the warming Indian Ocean and the western subtropical Pacific. Owing to the increased Indian-western Pacific warming and the prevalent CT La Niña events, the empirical seasonal forecast of SCSSM onset based on ENSO may be challenged in the future.

*Corresponding author: Congwen ZHU
Email: zhucw@cma.gov.cn

Key words: South China Sea summer monsoon onset, SCSSM, ENSO, cold tongue La Niña, seasonal forecast, monsoon onset

https://doi.org/10.1007/s00376-020-0090-y

Article Highlights:

- The past positive correlation between the SCSSM onset and ENSO became invalid during 2011-2019.
- The cold tongue (CT) La Niña delayed the SCSSM onset and broke the positive correlation.
- The empirical seasonal forecast of SCSSM onset may fail under future global warming

1. Introduction

The South China Sea (SCS) summer monsoon (SCSSM) onset generally occurs around 16 May. It has broadly been regarded as the prelude of East Asian summer monsoon rainy season (Tao and Chen, 1987; Lau and Yang, 1997; Wang et al., 2004; Zhu et al., 2005), and widely concerned in the sub-seasonal to seasonal (S2S) forecast in China (Zhu and Li, 2017). The crucial physical processes during the SCSSM onset are characterized by the eastward extension of the South Asian High (SAH) in the upper level (He et al., 1987; Liu and Zhu, 2016; Wei et al., 2019), eastward withdrawal of the western North Pacific subtropical high (WNPSH) (Xie et al., 1998; Wang et al., 2009), and the generation of convections and cross-equatorial flow over SCS (Gao and Xue, 2006; Hu et al., 2018).

ENSO has been regarded as the most important factor in the seasonal prediction of the SCSSM onset time on interannual timescale (Zhou and Chan, 2007; Luo et al., 2016; Luo and Lin, 2017; Martin et al., 2019). According to previous understanding, a warm (cold) ENSO event in winter tended to delay (advance) the onset of the SCSSM by strengthening (weakening) the WNPSH (Zhou and Chan, 2007). On decadal time scale, warming sea surface temperature (SST) in the equatorial western Pacific can cause the earlier SCSSM onset by enhancing intra-seasonal variability and tropical cyclone activities (Kajikawa and Wang, 2012), as well as the western Pacific warm pool heat content (Feng and Hu, 2014). However, the observed SCSSM onsets were relatively late in recent decade even though the observed SST keeps on warming over the equatorial western Pacific (Luo and Lin, 2017), particularly under a La Niña-like SST background (Liu and Zhu, 2019).

Here we found that the broken relationship between the SCSSM onset and ENSO can be attributed to the disturbance of cold tongue (CT) La Niña events. The prevalent CT La Niña events along with the Indian-western Pacific warming in recent decade could delay the SCSSM onset. Therefore, some previous empirical seasonal forecast models based on ENSO SST indices may fail due to the recently frequent CT La Niña events.

2. Data and Methods

The present study uses monthly and daily SST from the Hadley Centre Sea Ice and SST data set version 1 (HadISST1) with a 1°×1° grid (Rayner et al., 2003) and the National Oceanic and Atmospheric Administration (NOAA) High-resolution Blended Analysis of Daily SST (Reynolds et al., 2007), respectively. The NOAA interpolated daily outgoing longwave radiation (OLR) (Liebmann and Smith, 1996), and the monthly mean precipitation from the Climate Prediction Center (CPC) Merged Analysis of Precipitation (CMAP) with a spatial resolution of 2.5°×2.5° (Xie and Arkin, 1997) are also used. The daily and monthly atmospheric components are taken from the National Centers for Environmental Prediction/National Center for Atmospheric Research (NCEP/NCAR) reanalysis products (Kalnay et al., 1996) from 1948 to present, with a 2.5°×2.5° horizontal resolution. The mean seasonal cycle from 1981 to 2010 was removed to derive the anomalies for all the variables.

We, following Shao et al. (2014), define the SCSSM onset date by considering both the circulation and convection criteria. And the SCSSM onset date anomalies are referred to as the departure from the climatological onset date (May 16; reference line in Fig. 1a). The timing of SCSSM onset based on this definition is nearly consistent to the previous work (Shao et al., 2014), especially for the years to be analyzed (Wang et al., 2004; Liu et al., 2016; Liu and Zhu, 2019). Four ENSO indices (Niño 3.4, Niño 3, Niño 4, Niño 1+2) are used to access the relationship of ENSO diversity with SCSSM onset. Besides Pearson correlation, Spearman (Kendall) Rank correlation, namely intensity (phase) rank correlation, is used to evaluate the intensity (phase) correlation of ENSO with SCSSM onset. The Spearman Rank (intensity rank) correlation is simply the Pearson correlation coefficient computed using the ranks of the data in intensity. And Kendall (phase rank) correlation here is calculated by considering the matching relationship of the data pairs in phases, where the Niño indices and the SCSSM onset dates are classified into positive, negative and normal (0) categories.

3. Relationship between ENSO and SCSSM onset

The SCSSM onset shows a decadal variability, characterized by alternating late-onset (1979-1993 (P1) and 2011-2019(P3)) and early-onset (1994-2010 (P2)) periods during recent decades. The interdecadal change between P1 and P2 has been discussed in several studies (Kajikawa and Wang, 2012; Feng and Hu, 2014; Chen, 2015). It is suggested the relationship between the SCSSM onset and ENSO varies on decadal time scale (Wang et al., 2013; Ding et al., 2016; Liu et al., 2016). To examine whether the relationship between ENSO and SCSSM onset is stable or not, we calculated the correlations of SCSSM onset anomaly with four ENSO SST indices (Niño 4, Niño 3.4, Niño 3 and Niño 1+2) in previous winter (Fig. 1). The positive correlation during P2 is more notable than that during P1 (Fig. 1b), which seems to be attributed to the Atlantic Multidecadal Oscillation (AMO) or Pacific Decadal Oscillation (PDO) (e.g., Ding et al., 2016; Liu et al., 2016; Wang et al., 2017). However, the Pearson correlations of SCSSM onset with all Niño indices drop significantly during P3, suggesting the traditionally positive relationship between ENSO and SCSSM onset has been broken in recent decade.

The Pearson correlation between the SCSSM onset and ENSO indices is a result combining the mutual relationship of the intensities and phases between the two time series. The positive Pearson correlations between the SCSSM onset and ENSO indices during before 2010 (Fig. 1b) are mainly contributed by their phase correlation (Fig. 1c), instead of the intensity correlation (Fig. 1d). This implies that the influences of ENSO on SCSSM onset are mainly determined by the spatial pattern of El Niño-like or La Niña-like SST anomalies instead of the amplitude of ENSO indices (extreme or moderate). It is noted that the warm phase of ENSO is mostly followed by the late SCSSM onset during the whole period 1979-2019, but the cold phase of ENSO can be followed by either earlier or late onset (Fig. 1a). It has been suggested the notable positive correlation between ENSO and SCSSM onset during the early-onset period (P2) are attributed to the frequent La Niña event (Liu et al., 2016). However, the three cold events (2013, 2014 and 2018) during P3, corresponding to the negative phase of ENSO, are all followed by the late SCSSM onset. This suggests that the broken positive correlation between ENSO and SCSSM onset during P3 is possibly contributed by the negative phase of ENSO in recent decade.

To verify our hypothesis, we investigate five La Niña-like events (1999, 2000, 2001, 2008 and 2009) followed by notable early SCSSM onsets for comparison, and try to reveal the distinct impacts of cold ENSO between P2 and P3. Their composite SST anomalies in previous winter (DJF: December-January-February) resemble the canonical La Niña pattern (Fig. 2a) along with the strengthened pan-tropical Pacific

Walker circulation and the enhanced convection over the SCS (Fig. 2b). Two opposite anomalous vertical circular circulation centers are over the west and east of the SCS (Fig. 2b) with strong low-level zonal wind convergence over the SCS (Fig. 2a). The central-east Pacific cooling is likely related to the Bjerknes feedback, which emphasizes the role of the zonal wind in air-sea interaction.

Although the three cold events (2013, 2014 and 2018) in P3 share a similar anomalous SST morphology in P2 with the canonical La Niña events in rough, the detailed atmospheric circulation structures are quite different (Fig. 2c-2h vs. Fig. 2a-2b). The cooling areas in the east of the tropical Pacific for the three events are much narrower in the meridional direction (white boxes in Fig. 2c, 2e and 2g) along the equator, and their zonal trade wind anomalies around the dateline are much weaker. The equatorial narrow cooling in the three La Niña events is closely related to the surface meridional wind divergence instead of the zonal trade wind. In addition, the associated convections surrounding the eastern cooling regions are located in the western Pacific, north and south subtropical Pacific (Fig. 2c, 2e & 2g). Compared with the canonical La Niña events in Fig. 2a & 2b, the convections in the recent three cold events are much weaker and located in the east of the SCS. Correspondingly, a strong vertical circular circulation is located on the east of 150°E. Some scattered convections around the SCS also induce several reversed vertical circular circulations, but seem irrelevant to the large-scale Pacific Walker circulation (Fig. 2d, 2f & 2h). Considering the common unique features of the three cold events, these La Niña-like events along with surface meridional wind divergence and narrow east cooling resembles the so-called cold tongue (CT) mode (Zhang et al., 2010; Li et al., 2015; Jiang and Zhu, 2018,2020), namely a background mode under recent global warming. Therefore, these cold events in P3 can be named as cold tongue (CT) La Niña events. However, it is hard to distinguish these CT La Niña events from the canonical La Niña events only based on the current SST Niño indices. Then a new index is introduced to depict the CT La Niña events.

Considering the surface wind features of CT La Niña events, the surface meridional wind divergence ($\frac{\partial v}{\partial y}$) averaged within the box in Fig. 2c, namely MD_c index, is used to depict the variation related to the CT La Niña events. However, the strengthened zonal winds for the canonical La Niña events within the box (U_w index) in Fig. 2a can also induce meridional wind divergence sometimes (Fig. 2i). On the other hand, compared with canonical La Niña events followed by early SCSSM onsets (marked in blue dots), the zonal trade winds (U_w) in the CT La Niña events (marked in red dots) are much weaker. It seems that both strengthened zonal trade wind and the surface meridional wind divergence can uplift the thermocline and cool the SST in the east Pacific. To address the CT La Niña dominated by $\frac{\partial v}{\partial y}$, the residual MD_c is obtained by linearly removing the influence of the U_w index. Fig. 2j illustrates the time series of the observed Niño 3.4 index and that regressed on the residual MD_c and the combination of the residual MD_c and U_w index. Results show that Niño 3.4 index regressed on the combination of the residual MD_c and U_w index gives a times series more correlated with the observed Niño 3.4 index (Mean Squared Error (MSE): 0.12) than that regressed on the residual MD_c alone (MSE:0.67). However, the Niño 3.4 indices of the three CT La Niña events are well reproduced by the residual MD_c (MSE: 0.016) in recent decade, suggesting the dominant role of the meridional wind divergence in inducing eastern Pacific cooling of the recent three CT La Niña events. Therefore, the residual MD_c is used as an index to depict the CT La Niña events. Since there are distinct differences between the CT La Niña events and the canonical ones, their impacts on the pre-onset stage of the SCSSM onset are further examined.

4. Impact of cold tongue La Niña events on SCSSM onset

The persistence of SST anomalies (SSTA) and the circulation patterns from previous winter to spring may keep the ENSO-SCSSM linear relationship and favor the seasonal forecast of the SCSSM onset (Fig. 3a–f). Fig. 3 shows the time evolution of air-sea anomalies (OLR and SSTA) before the SCSSM onset for each cold event during P2 and P3. The five La Niña events followed by early SCSSM onsets in P2 exhibit persisting enhanced convection over the SCS from winter to spring (April) favoring the early onset of the SCSSM (marked by black circles in Fig. 3a–f). In contrast, no obvious persisting enhanced convection signals are observed in SCS following the CT La Niña events in P3, and the suppressed convections over the SCS in May postponed the SCSSM onsets.

Being consistent with the persistence of convection over the SCS, the air-sea structures of the canonical La Niña events during P2 also persist from winter to spring (Fig. 4a-

4c). However, the structures of the CT La Niña events change a lot in spring. An evident anomalous anticyclone (marked by letter “A” in the left column in Fig. 4) in lower troposphere is centered over the SCS with suppressed convection, which possibly postpone the SCSSM onset. The enhanced convections surrounding the SCS are mainly located over the northern Indian Ocean, Maritime Continents and the western Pacific (150°E-180°), inducing vertical circular circulations influencing the SCSSM onset. For instance, in May 2013, the enhanced convections over the Maritime Continents and northern Indian Ocean induce strong descending motion over the SCS (the second row in Fig. 4). Besides the convections over the Maritime Continents and the northern Indian Ocean, the enhanced convections over the northern subtropical Pacific also suppress the convections over the SCS in 2018 (the last row in Fig. 4).

According to the above analyses, the canonical La Niña events in P2 strengthen the pan-tropical Pacific Walker circulation, enhance persisting convection over the SCS and advance the SCSSM onset, supporting the positive relationship between SCSSM onset and ENSO. In contrast, the CT La Niña events in P3 induce a vertical circular circulation over east of the SCS, but it cannot maintain to spring. The late onset of the SCSSM following the CT La Niña years in P3 are mainly postponed by enhanced convections over the northern Indian Ocean, the Maritime Continent and the western Pacific surrounding the SCS.

To further verify the impact of the CT La Niña event on the late SCSSM onset, we firstly remove the influence of the zonal wind (U_w), and then indicate the variations of the CT La Niña events by the DJF residual MD_c index. By regressing SST anomalies on the DJF residual MD_c index, the winter (DJF) SST anomalies pattern resembles that of the three CT La Niña events, featured by a narrow cooling in the east equatorial Pacific along with significant meridional wind divergence (Fig. 5a). In addition, there is slight cooling over the Indian Ocean and the oceans surrounding the Maritime Continent.

The warming Indian Ocean-western Pacific and the cooling along the coast of Peru in the CT La Niña events during P3 are mainly contributed by their trends under global warming (Fig. 5b). And the northern and southern subtropical Pacific are warming significantly via the wind-evaporation-sea surface temperature (WES) feedback (Fig. 5a). Considering the seasonal march of the warm pool regions (purple lines in Fig. 5a & 5c) and the evolutions of the CT La Niña event, the convections over the SCS should be suppressed thanks to the enhanced convections surrounding, particularly over the Indian Ocean and the northern subtropical Pacific.

Besides the interannual variation, the warming trend of the Indian Ocean (IO) is also significant. Although the IO Capacitor effect (Xie et al., 2009) after ENSO can still be detected by the phase-lag relationship of SSTA between the eastern Pacific (EP) and IO (Fig. 5e), the SSTA can hardly get cooled due to the rapid warming in IO in recent decade, suggesting an asymmetrical response of IO SSTA to ENSO. For three CT La Niña events during P3, the warming surrounding the SCS could enhance convections and postpone the SCSSM onset, Since the SCSSM onset can be also triggered by the synoptic or intra-seasonal activities, the warming SST in IO can enhance convection and atmospheric disturbance and in turn bring greater uncertainties for the seasonal forecast of SCSSM onset. Following an El Niño event, the warming SSTA could become remarkable in IO, and result in enhanced convection disturbances to trigger an early onset of the SCSSM. For example, the extreme early SCSSM onset in 2019 is attributed to the intra-seasonal oscillation (Hu et al., 2020) and typhon "Fani" (Liu and Zhu, 2020). Liu and Zhu (2020) indicated that the anomalous condensation heating released by the typhon "Fani" not only shifted the South Asian High (SAH) northward but also reinforced the upper-level barotropic trough to the west of the Tibetan Plateau (TP) at midlatitudes. It facilitated the early establishment of monsoon convection by intensifying the upper-level pumping over the SCS.

5. Summary and discussion

ENSO has been treated as the most important predictor for the SCSSM onset in the empirical and dynamical model (Zhu and Li, 2017; Martin et al., 2019). A warm (cold) ENSO event is often followed by the late (early) onset of SCSSM. However, this positive correlation does not work during 2011-2019. Our results show the anomaly of SCSSM onset is mainly determined by the phases (warm or cold) of ENSO, instead its amplitude of anomalous SST index. The recently invalid positive correlation of SCSSM onset with ENSO can be attributed to the disturbance of cold tongue (CT) La Niña events during 2011-2019.

The anomalous SST morphology of the CT La Niña resembles the conventional ones, but its cooling area is narrowed along the equator with weaker trade winds. We found that the cooling SST of CT La Niña events are dominated by the meridional wind divergence in the eastern Pacific, this is distinct from the canonical (?) La Niña events with strong trade winds. Following the CT La Niña in preceding winter, the suppressed convections over the SCS in May postpone the SCSSM onset, which is mainly due to the enhanced convections over the northern Indian Ocean, the western Pacific as well as the Maritime Continent. It is suggested that both the evolution of the CT La Niña and the warming SST in the Indian-western Pacific contribute to the late SCSSM onset. The CT La Niña events dominated by the surface meridional wind divergence more likely occur in recent years, and is hardly distinguished from the canonical ones by the SST ENSO indices alone. Due to the distinct influences of the CT La Niña events, some known empirical seasonal forecast models based on ENSO SST indices may be challenged. Therefore, besides these SST ENSO indices, the additional indices, such as U_w and MD_c, are also suggested to be used to monitor ENSO issues for the seasonal forecast of SCSSM onset. The increasing CT La Niña events may also affect the ENSO diversity including the SST patterns and evolutions. Hence more studies should be carried on for understanding the CT La Niña events.

Acknowledgments. The author acknowledges the anonymous reviewers' helpful suggestions and Dr. Jeremy Cheuk-Hin Leung's polishing. This work was jointly sponsored by the National Science Natural Foundation of China (41830969), the

National Key R&D Program (2018YFC1505904), and the Basic Scientific Research and Operation Foundation of the CAMS (2018Z006 and 2018Y003). This study was also supported by the Jiangsu Collaborative Innovation Center for Climate Change.
The HadISST1 data set was obtained from the Met Office Hadley Centre and can be downloaded from http://www.metoffice.gov.uk/hadobs/hadisst/data/download.html. NOAA High-resolution Blended Analysis of Daily SST, NCEP reanalysis data, interpolated OLR data and CMAP precipitation data provided by the NOAA/OAR/ESRL PSD, Boulder, Colorado, USA can be obtained from their website at https://www.esrl.noaa.gov/psd/.

REFERENCES

Chen, G., 2015: Comments on "Interdecadal change of the South China Sea Summer Monsoon Onset". Journal of Climate, 28, 9029-9035.

Ding, S., Z. Wen, and W. Chen, 2016: Interdecadal change in the relationship between the South China Sea summer monsoon onset and two types of pacific sea surface temperature anomaly. Chinese Journal of Atmospheric Sciences, 40, 243-256.

Feng, J., and D. Hu, 2014: How much does heat content of the western tropical Pacific Ocean modulate the South China Sea summer monsoon onset in the last four decades? Journal of Geophysical Research: Oceans, 119, 4029-4044.

Gao, H., and F. Xue, 2006: Seasonal variation of cross-equatorial flow and their influences on the onset of the South China Sea Summer Monsoon. Climatic and Environmental Research, 11, 57-68.

He, H., J. W. McGinnis, Z. Song, and M. Yanai, 1987: Onset of the Asian Summer Monsoon in 1979 and the Effect of the Tibetan Plateau. Monthly Weather Review, 115, 1966-1995.

Hu, P., W. Chen, R. Huang, and D. Nath, 2018: On the weakening relationship between the South China Sea summer monsoon onset and cross-equatorial flow after the late 1990s. International Journal of Climatology, 38, 3202-3208.

Hu, P., W. Chen, S. Chen, Y. Liu, and R. Huang, 2020: Extremely early summer monsoon onset in the South China Sea in 2019 following an El Niño event. Monthly Weather Review.

Jiang, N., and C. Zhu, 2018: Asymmetric Changes of ENSO Diversity Modulated by the Cold Tongue Mode Under Recent Global Warming. Geophysical Research Letters, 45, 12,506-512,513.

Jiang, N., and C. Zhu, 2020: Tropical Pacific cold tongue mode triggered by enhanced warm pool convection due to Global Warming. Environmental Research Letters.

Kajikawa, Y., and B. Wang, 2012: Interdecadal Change of the South China Sea Summer Monsoon Onset*. Journal of Climate, 25, 3207-3218.

Kalnay, E., and Coauthors, 1996: The NCEP/NCAR 40-Year Reanalysis Project. Bulletin of the American Meteorological Society, 77, 437-471.

Lau, K. M., and S. Yang, 1997: Climatology and interannual variability of the Southeast Asian summer monsoon. Advances in Atmospheric Sciences, 14, 141-162.

Li, Y., J. Li, W. Zhang, X. Zhao, F. Xie, and F. Zheng, 2015: Ocean dynamical processes associated with the tropical Pacific cold tongue mode. Journal of Geophysical Research: Oceans, 120, 6419-6435.

Liebmann, B., and C. A. Smith, 1996: Description of a Complete (Interpolated) Outgoing Longwave Radiation Dataset. Bulletin of the American Meteorological Society, 77, 1275-1277.

Liu, B., and C. Zhu, 2016: A possible precursor of the South China Sea summer monsoon onset: Effect of the South Asian High. Geophysical Research Letters, 43, 11,072-011,079.

Liu, B., and C. Zhu, 2019: Extremely late onset of the 2018 South China Sea summer monsoon following a La Niña event: Effects of triple SST anomaly mode in the North Atlantic and a weaker Mongolian cyclone. Geophysical Research Letters, 46.

Liu, B., and C. Zhu, 2020: Boosting Effect of Tropical Cyclone “Fani” on the Onset of the South China Sea Summer Monsoon in 2019. Journal of Geophysical Research: Atmospheres, 125, 1-16.

Liu, B., C. Zhu, Y. Yuan, and K. Xu, 2016: Two types of interannual variability of South China sea summer monsoon onset related to the SST anomalies before and after 1993/94. Journal of Climate, 29, 6957-6971.

Luo, M., and L. Lin, 2017: Objective determination of the onset and withdrawal of the South China Sea summer monsoon. Atmospheric Science Letters, 18, 276-282.

Luo, M., Y. Leung, H. F. Graf, M. Herzog, and W. Zhang, 2016: Interannual variability of the onset of the South China Sea summer monsoon. International Journal of Climatology, 36, 550-562.

Martin, G. M., A. Chevuturi, R. E. Comer, N. J. Dunstone, A. A. Scaife, and D. Zhang, 2019: Predictability of South China Sea Summer Monsoon Onset. Advances in Atmospheric Sciences, 36, 253-260.

Rayner, and Coauthors, 2003: Global analyses of sea surface temperature, sea ice, and night marine air temperature since the late nineteenth century. Journal of Geophysical Research, 108, 4407-4407.

Reynolds, R. W., T. M. Smith, C. Liu, D. B. Chelton, K. S. Casey, and M. G. Schlax, 2007: Daily high-resolution-blended analyses for sea surface temperature. Journal of Climate, 20, 5473-5496.

Shao, X., P. Huang, and R. H. Huang, 2014: Role of the phase transition of intraseasonal oscillation on the South China Sea summer monsoon onset. Climate Dynamics, 125-137.

Tao, S., and L. Chen, 1987: A review of recent research on the East Asia summer monsoon in China. Monsoon Meteorology, C. P. Chang, and T. N. Krishnamurti, Eds., Oxford Univ. Press, 60-92.

Wang, B., LinHo, Y. Zhang, and M. M. Lu, 2004: Definition of South China Sea monsoon onset and commencement of the East Asian summer monsoon. Journal of Climate, 17, 699-710.

Wang, B., F. Huang, Z. Wu, J. Yang, X. Fu, and K. Kikuchi, 2009: Multi-scale climate variability of the South China Sea monsoon: A review. Dynamics of Atmospheres and Oceans, 47, 15-37.

Wang, X., X. Jiang, S. Yang, and Y. Li, 2013: Different impacts of the two types of El Niño on Asian summer monsoon onset. Environmental Research Letters, 8. DOI: 10.1088/1748-9326/8/4/044053

Wang, L., J. Y. Yu, and H. Paek, 2017: Enhanced biennial variability in the Pacific due to Atlantic capacitor effect. Nature Communications, 8, 1-7.

Wei, W., Y. Wu, S. Yang, and W. Zhou, 2019: Role of the South Asian High in the Onset Process of the Asian Summer Monsoon during Spring-to-Summer Transition. Atmosphere, 10, 239.

Xie, A., Y.-S. Chung, X. Liu, and Q. Ye, 1998: The Interannual Variations of the Summer Monsoon Onset overthe South China Sea. Theoretical and Applied Climatology, 59, 201-213.

Xie, P., and P. A. Arkin, 1997: Global Precipitation: A 17-Year Monthly Analysis Based on Gauge Observations, Satellite Estimates, and Numerical Model Outputs. Bulletin of the American Meteorological Society, 78, 2539-2558.

Xie, S. P., K. Hu, J. Hafner, H. Tokinaga, Y. Du, G. Huang, and T. Sampe, 2009: Indian Ocean capacitor effect on Indo-Western pacific climate during the summer following El Niño. Journal of Climate, 22, 730-747.

Zhang, W., J. Li, and X. Zhao, 2010: Sea surface temperature cooling mode in the Pacific cold tongue. Journal of Geophysical Research: Oceans, 115, C12042.

Zhou, W., and J. C. L. Chan, 2007: ENSO and the South China Sea summer monsoon onset. International Journal of Climatology, 27, 157-167.

Zhu, C., W.-S. Lee, H. Kang, and C.-K. Park, 2005: A proper monsoon index for seasonal and interannual variations of the East Asian monsoon. Geophysical Research Letters, 32, L02811.

Zhu, Z., and T. Li, 2017: Empirical prediction of the onset dates of South China Sea summer monsoon. Climate Dynamics, 48, 1633-1645.

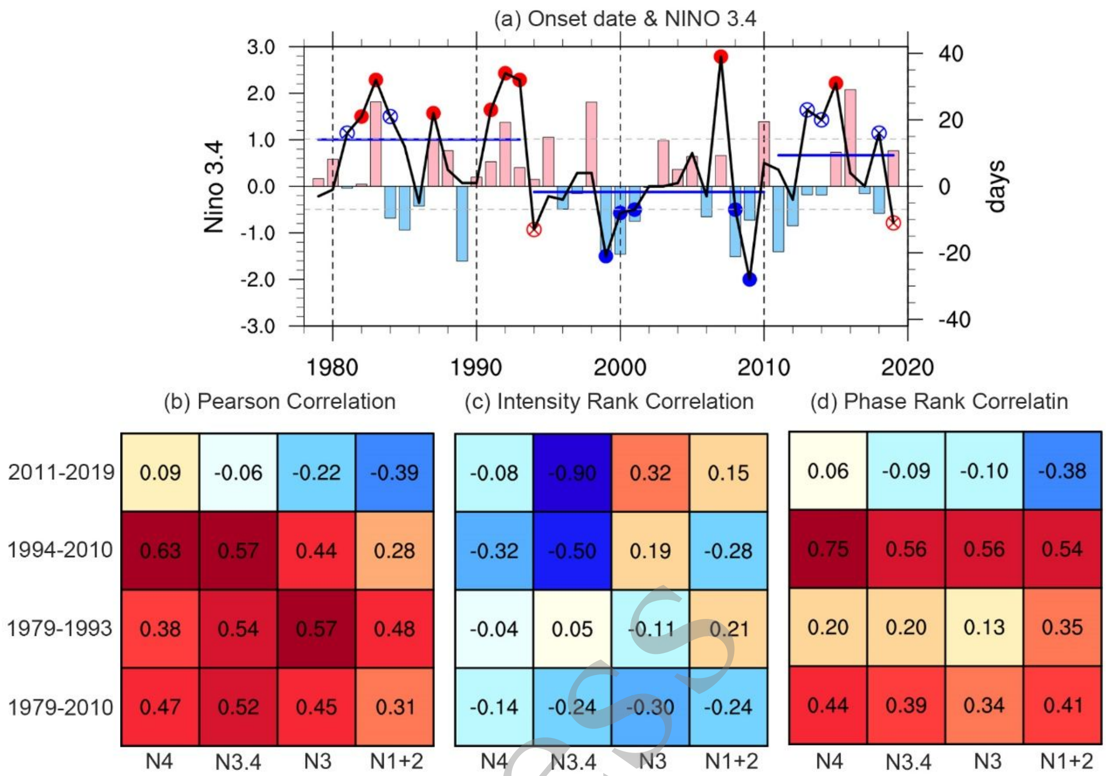

Fig. 1. (a) Time series of the SCSSM onset date anomalies and the DJF Niño 3.4 index (bars). The two horizontal dashed lines represent the averaged values for the late and early onset date anomalies respectively. The SCSSM onset dates exceeding the dashed lines are marked by the dots and circles. The red (blue) dots indicate a late (an early) onset with a positive (negative) Niño 3.4 index in previous winter, and instead the others with a reverse relationship are marked by the circles. The blue lines illustrate the averaged onset dates for the periods of 1979—1994, 1995—2010 and 2011—2019. (b-d) Correlation coefficients between four ENSO indices and SCSSM onset date during the three periods. The Pearson correlation, Intensity Rank correlation and Phase Rank correlation are illustrated in (b), (c) and (d), respectively.

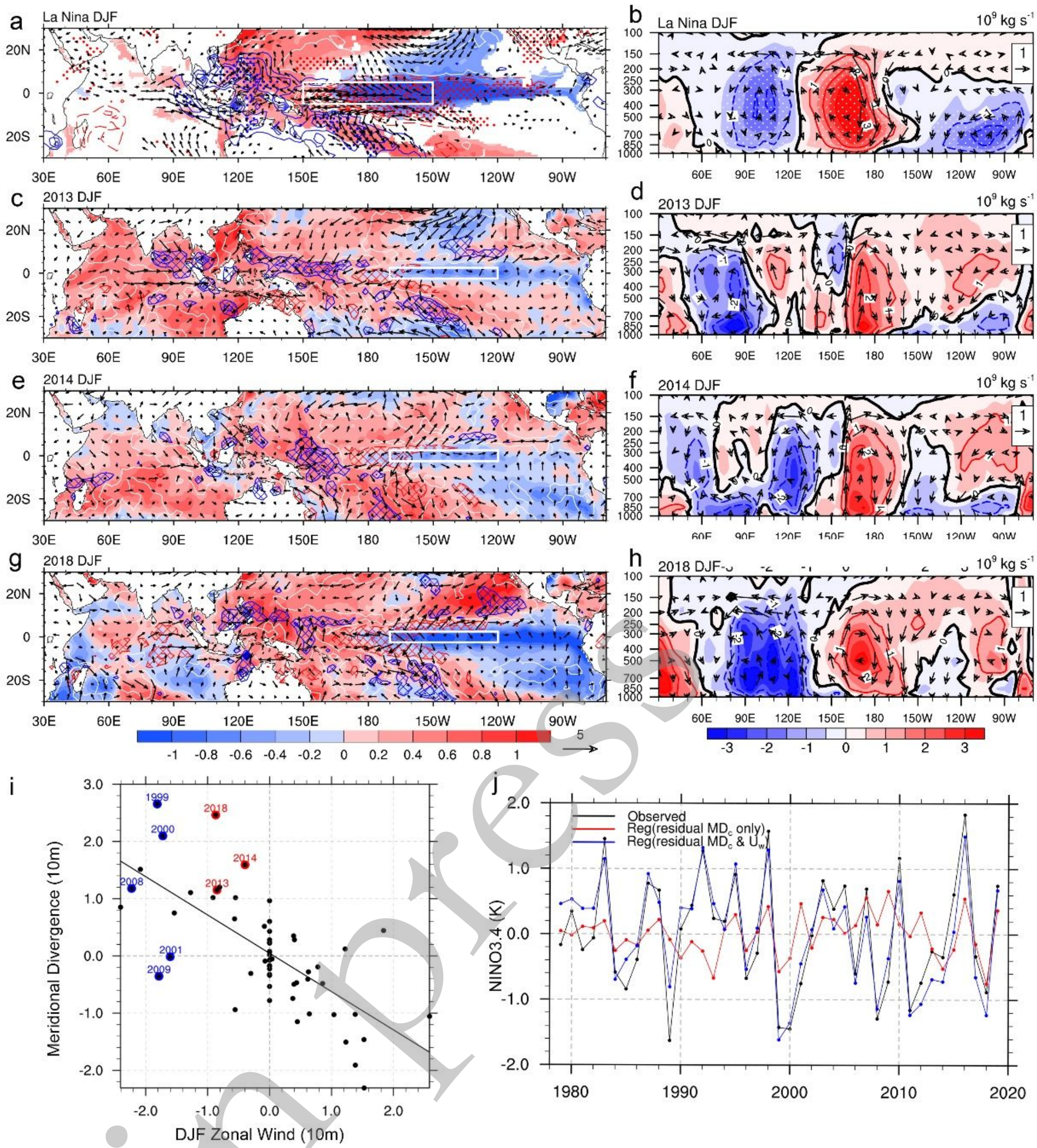

Fig. 2. (a) DJF SST (shading), 10-m wind (vector) and precipitation anomalies (contour; blue: positive, red: negative), and (b) zonal mass stream function, pressure velocity (omega× -50; Pa/s), and zonal divergent wind (m/s) averaged within 5°S −5°N for the composited La Niña event (1999, 2000, 2001, 2008 and 2009). The second, third and fourth rows represent those in 2013, 2014 and 2018 (precipitation anomalies: contour with crossing lines, 2 mm/day interval). Only the values for the wind and SST

(precipitation) anomalies above the 90% confidence level are shown (marked by dots) in (a). The white boxes in (a) and (c) represent the areas that define U_w and MD_c indices, respectively. (i) Scatterplot of U_w and MD_c for winters (DJF) from 1979 to 2019. Blue dots represent the La Niña events followed by early SCSSM onset. 2013, 2014 and 2018 cases with late SCSSM onset are shown as red dots. (j) shows the time series of DJF Niño 3.4 index: (gray) observations, (red) linear regression with the residual MD_c as the only predictor, and (blue) linear regression with both the U_w and residual MD_c indexes as predictors.

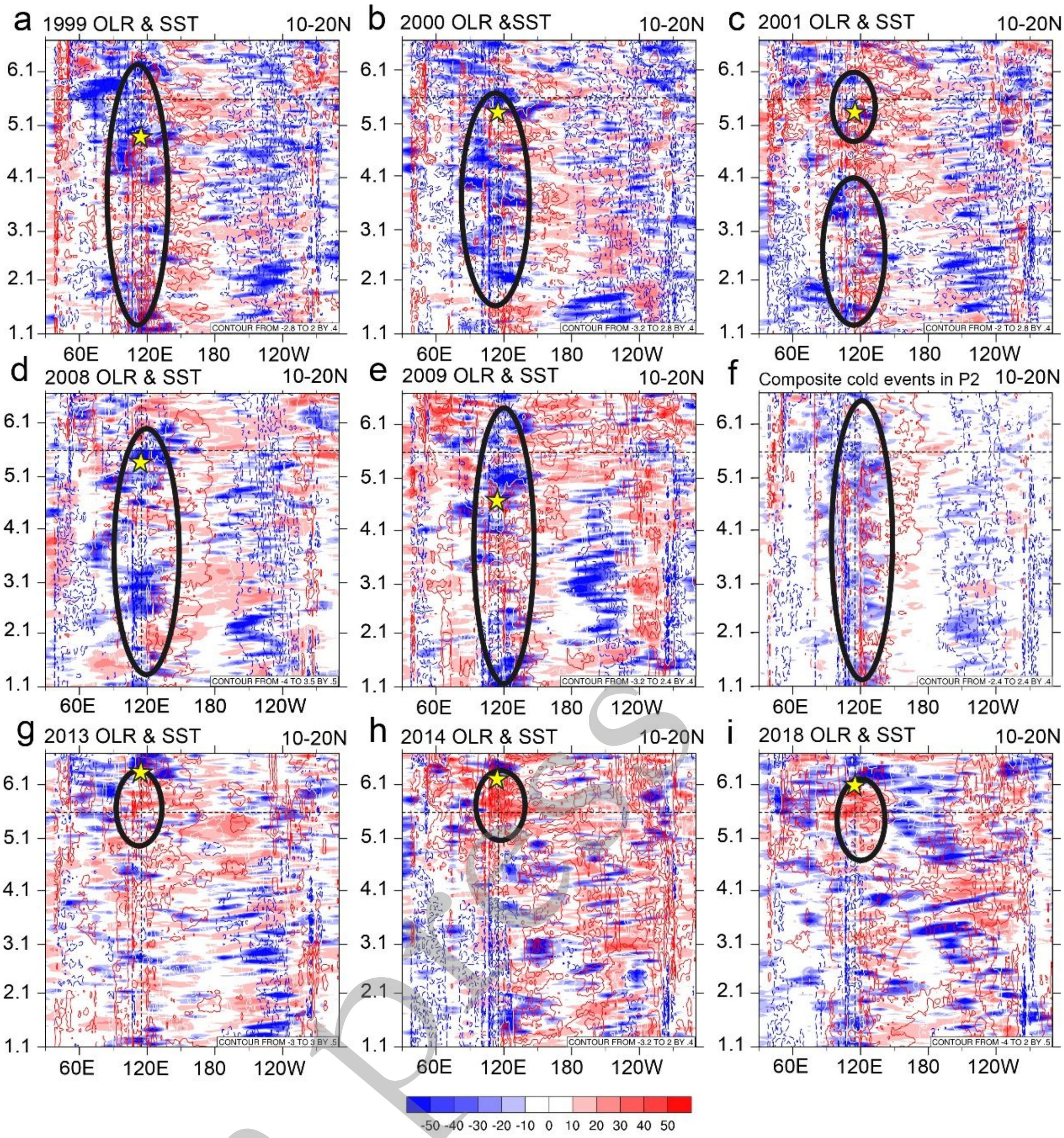

Fig. 3. Hovmoller diagrams for OLR (shading) and SST (contours; red (blue): positive (negative)) anomalies averaged within the tropical band (10°N−20°N) for composited (f) and individual cases. (f) represents the case composited by (a-e). The horizontal and vertical reference lines represent the climatological SCSSM onset date and the SCS position. The yellow stars indicate the SCSSM onset dates for different years.

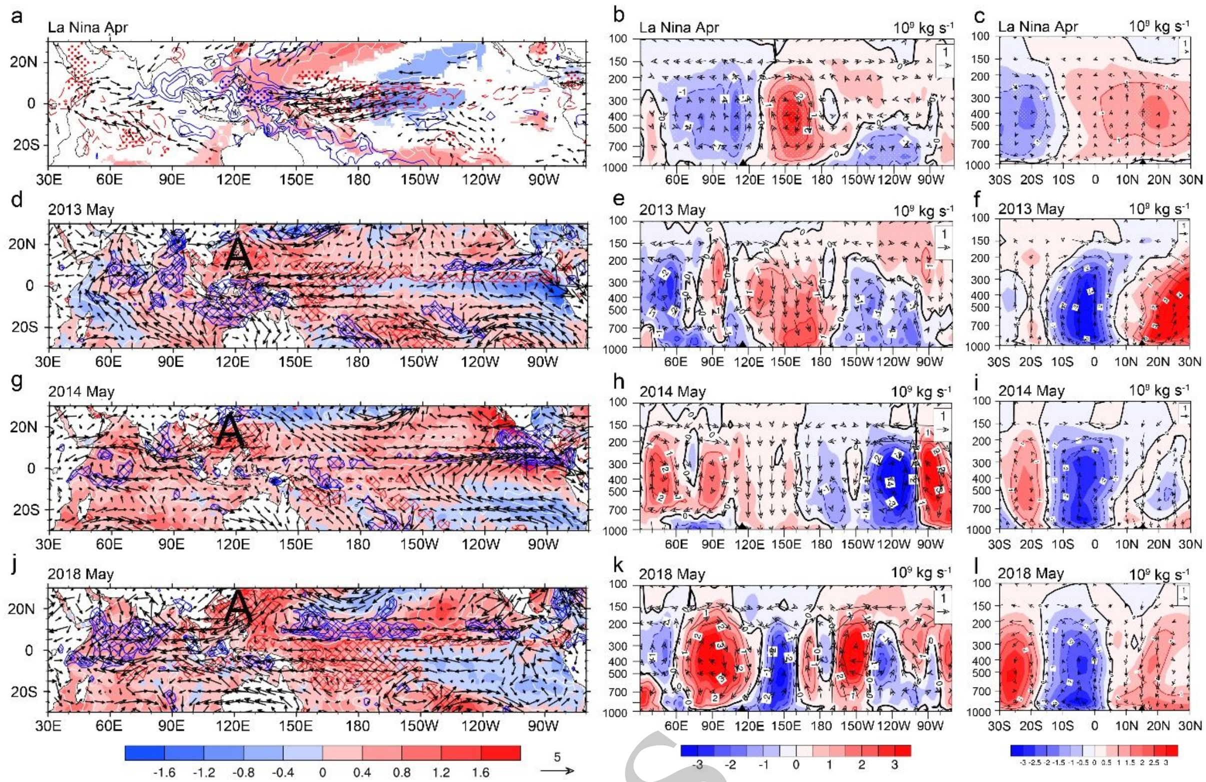

Fig. 4. Similar as Fig. 2. (a) SST (shading), 10-m wind (vector) and precipitation (contour; blue: positive, red: negative) anomalies, (b) zonal mass stream function, pressure velocity (omega× -50; Pa/s), and zonal divergent wind (m/s) averaged within 10−20°N, (c) meridional mass stream function, pressure velocity (omega× -50; Pa/s), and meridional divergent wind (m/s) averaged within 110−120°N for the composited La Niña case in May. The second, third and fourth rows represent those in 2013, 2014 and 2018. The location of the SCS is marked by black triangle in the last two rows.

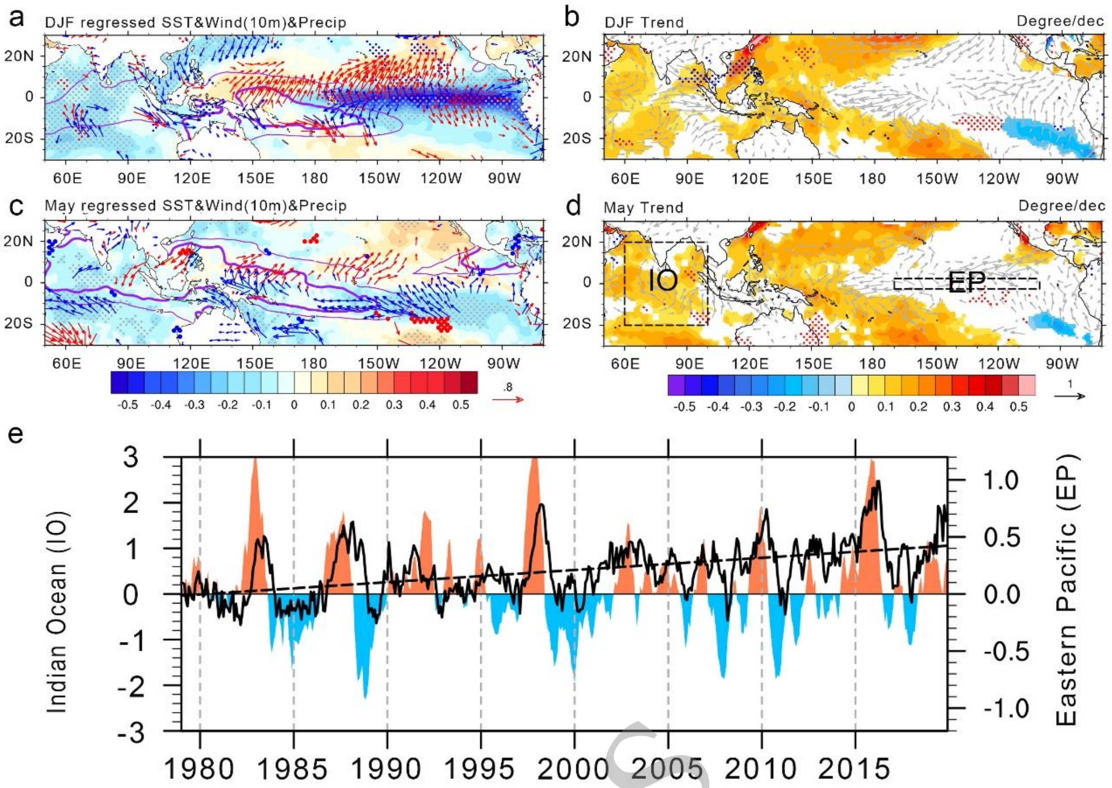

Fig. 5. (a) The DJF residual MD_c-regressed (a) DJF and (c) May SSTA spatial distribution (shading; 0.05 K interval), horizontal wind at 10m (vectors), and precipitation (dots; mm day^{-1}). The blue (red) dots indicate the positive (negative) precipitation anomalies. The surface wind anomalies strengthen (weaken) climatological winds are in blue (red). The thin and thick purple lines indicate the climatological 28 and 29℃ isotherms in (a) DJF and (c) May. Trends in SST (℃ dec^{-1}), 10m winds (arrows (m s^{-1} dec^{-1})), and precipitation (blue (red) dots: positive (negative)) for (b) DJF and (d) May, respectively. (e) SSTA averaged within the Indian Ocean (IO: black solid line) and Eastern Pacific (EP: blue and red shading) regions (marked in (d)), and the dashed line indicates the linear trend for the time series of the IO SSTA.